

Molecular Approach to the Mechanism of Deposition–Precipitation of the Ni(II) Phase on Silica

Paolo Burattin,[†] Michel Che,[‡] and Catherine Louis*

Laboratoire de Réactivité de Surface, URA 1106 CNRS, Université P. et M. Curie, 4 place Jussieu, 75252 Paris Cedex 05, France

Received: October 29, 1997

A molecular mechanism explaining the chemical phenomena that occur during the preparation of silica-supported nickel catalysts by the method of deposition–precipitation is proposed. This mechanism takes into account the fact that either 1:1 nickel phyllosilicate or nickel hydroxide may be formed on silica during deposition–precipitation, depending on the silica surface area and the deposition–precipitation time, as shown in our previous paper (Burattin, P.; Che, M.; Louis, C. *J. Phys. Chem. B* **1997**, *101*, 7060). The mechanism is mainly based on the kinetic competition between two types of reactions: (i) Ni–O–Si heterocondensation/polymerization, which leads to the growth of 1:1 nickel phyllosilicate on a Ni(II) brucitic layer bonded to silica; (ii) Ni–OH–Ni olation/polymerization, which leads to the formation and the growth of nickel hydroxide on a Ni(II) brucitic layer bonded to silica. The former type of reaction is faster than the latter but is limited by the concentration in solution of silicic acid arising from silica dissolution and by its diffusion rate. The changes in the pH curves, the yield of Ni(II) deposition–precipitation, and the nature of the supported Ni(II) phase during deposition–precipitation under different experimental conditions are also interpreted on the basis of the mechanism proposed.

I. Introduction

A few years ago, Geus et al.^{1–3} developed a new method to prepare supported catalysts, called deposition–precipitation. This method is a modification of the precipitation methods in solution. Practically, the preparation of Ni/SiO₂ catalysts by deposition–precipitation consists of the precipitation of nickel onto the silica surface by basification of a nickel salt solution. The key factor of this preparation is the basification by gradual and homogeneous addition of hydroxide ions throughout the whole solution, to avoid local supersaturations and the precipitation of nickel hydroxide in solution. The use of urea (CO(NH₂)₂) rather than that of sodium hydroxide is advised because solution mixing and basification can be performed in two separate steps: urea is mixed to the solution at room temperature, and urea hydrolysis starts when the mixture is heated to 90 °C; hydroxide ions are homogeneously generated within the solution, and precipitation only takes place onto the support because of the interaction between the nickel(II) species and silica.

The approach of Geus et al.^{3,4} to interpret the mechanism of deposition–precipitation (DP) may be considered as a kinetic and thermodynamic approach of the nucleation and growth of the DP Ni(II) phase onto the silica support. According to the authors,^{3,4} if one considers the phase diagram of a solid in equilibrium with a solution (Figure 1), the solubility curve (s) corresponds to the equilibrium curve separating the monophasic domain from the biphasic one, but nucleation and precipitation occurs when the concentration reaches the curve of supersolubility (ss). The addition of a precipitating species usually does not keep up with the consumption of the precipitant by the

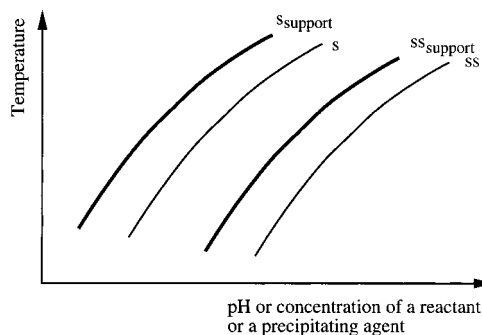


Figure 1. Phase diagram for a pure solution (solid lines) and in the presence of a support (bold lines).

rapidly growing nuclei, so that the concentration of the precipitating species passes through a maximum. For example, when OH[−] is the precipitating species, a maximum of pH is reached. In the presence of a finely divided support suspended in the solution, both the solubility (*s*_{support}) and the supersolubility curves (*ss*_{support}) are shifted to lower concentration (Figure 1), provided that the ions of the active species in solution can chemically interact with the surface of the support. According to Hermans and Geus,³ the interaction decreases the nucleation barrier as long as nucleation at the surface of the support can proceed at a concentration between the solubility and the supersolubility curves. So, at concentrations between those of the supersolubility curves, *ss*_{support} and *ss*, the compound exclusively precipitates onto the support surface. It may be added that according to Geus,⁴ the difference in concentrations between the two supersolubility curves, *ss*_{support} and *ss*, is related to the bond strength between the precipitate and the support surface.

In a previous paper,⁵ we have shown that the nature of the DP Ni(II) phase depends on the silica surface area and the DP

[†] Permanent address: Rhône Poulenc CRIT-Carières, 86 avenue des Frères Perret, BP 62, 69192 Saint Fons Cedex, France.

[‡] Institut Universitaire de France.

TABLE 1: Influence of the Silica Surface Area and the DP Time on the Nature of the Ni(II) Phase

silica		DP time	nature of the Ni(II) phase ^a	remarks
surface area	origin			
low ($\approx 50 \text{ m}^2\cdot\text{g}^{-1}$)	XO30LS	$\leq 4 \text{ h}$	supported nickel hydroxide	aging period: crystallinity increases with DP time
		4–16 h	supported 1:1 nickel phyllosilicate	
		$> 16 \text{ h}$	bulk 1:1 nickel phyllosilicate	
high ($\approx 400 \text{ m}^2\cdot\text{g}^{-1}$)	XOA400	$\leq 100 \text{ min}$	supported 1:1 nickel phyllosilicate with small amount of supported nickel hydroxide	aging period: crystallinity increases with DP time; lower crystallinity than on XO30LS
		100 min–16 h	supported 1:1 nickel phyllosilicate	
		$> 16 \text{ h}$	bulk 1:1 nickel phyllosilicate	

^a 2:1 nickel phyllosilicate is only formed after hydrothermal treatment

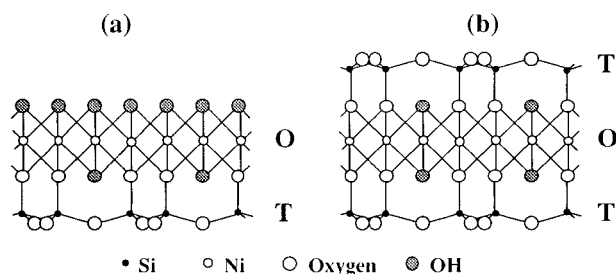


Figure 2. Projection on the *bc* plane of (a) a TO layer of 1:1 nickel phyllosilicate; (b) a TOT layer of 2:1 nickel phyllosilicate, from ref 23.

time (Table 1); on silica of low surface area ($\approx 50 \text{ m}^2\cdot\text{g}^{-1}$) and after short DP time ($\leq 4 \text{ h}$), the DP Ni(II) phase is mainly a turbostratic nickel hydroxide, $\alpha\text{-Ni}(\text{OH})_2$, i.e., a nickel hydroxide with a disordered stacking of the brucitic layers of octahedral Ni(II).⁶ The layers in the DP nickel hydroxide are separated by intercalated nitrate and isocyanate anions. For longer DP times, the DP Ni(II) phase is mainly a 1:1 nickel phyllosilicate with nitrate and isocyanate anions entrapped in the structure. Like $\alpha\text{-Ni}(\text{OH})_2$, 1:1 nickel phyllosilicate exhibits a layered structure consisting of a brucite-type sheet containing Ni(II) in octahedral coordination and a sheet containing linked tetrahedral SiO₄ units (Figure 2a). In the presence of silica of high surface area ($\approx 400 \text{ m}^2\cdot\text{g}^{-1}$), the DP Ni(II) phase is a 1:1 nickel phyllosilicate with a small proportion of turbostratic nickel hydroxide for very short DP time ($\leq 100 \text{ min}$). For longer DP time, the DP Ni(II) phase is a 1:1 nickel phyllosilicate of increasing crystallinity. The formation of 1:1 nickel phyllosilicate was also observed in former works dealing with the Ni(II) deposition–precipitation on silicas of high surface area.^{2,3,7} For very long DP time ($\geq 16 \text{ h}$), silica is totally consumed and bulk 1:1 nickel phyllosilicate is obtained.⁵

To complement the results obtained in our previous paper,⁵ the influence of several parameters of preparation of Ni/SiO₂ samples will be examined: the concentrations of urea and of nickel nitrate and the silica loading. In particular, the curves of pH, recorded during deposition–precipitation under these different conditions, are presented.

The goal of this paper is to propose a molecular approach to the mechanism of deposition–precipitation of Ni(II) on silica, which takes into account the formation of DP Ni(II) phases of different natures. This approach will be compared to the kinetic and thermodynamic approach proposed by Geus et al.^{3,4}

II. Experimental Section

1. Sample Preparation. The standard conditions used to prepare the DP Ni/SiO₂ catalysts whose results are described in Section III.2.a are the same as in ref 3: 380 mg of silica or

other support was put into a vessel thermostated at 90 °C. Fifty milliliters of an aqueous solution containing nickel nitrate (0.14 M), urea (0.42 M), and nitric acid (0.02 M) were added at $t = 0$, and the suspension ($7.6 \text{ g}\cdot\text{L}^{-1}$ of silica) was magnetically stirred. Addition of nitric acid allows strong changes in pH at the beginning of basification. Reactant concentrations differing from standard conditions will be used in Sections III.2.b–d. In any case, the solution reached 90 °C within 3 min, and the deposition–precipitation started. Changes in pH of the solution were plotted versus the DP time up to 150 min. The pH began to be recorded after $t = 10 \text{ min}$ because of the problem of electrode equilibrium. After 150 min of deposition–precipitation, the suspension was cooled to 20–25 °C and then filtered. The sample was washed three times; after addition of 20 mL of distilled water, the suspension was stirred for 10 min at 50–60 °C before filtration. Finally, the sample was dried at 90 °C for 24 h and characterized.

The samples were prepared with porous silicas Spherosil (Rhône-Poulenc, France, purity $> 99.5\%$) XOA400 ($S_{\text{BET}} = 356 \text{ m}^2\cdot\text{g}^{-1}$, pore volume = $1.25 \text{ cm}^3\cdot\text{g}^{-1}$, average pore diameter = 80 Å) and XO30LS ($S_{\text{BET}} = 44 \text{ m}^2\cdot\text{g}^{-1}$, pore volume = $2.27 \text{ cm}^3\cdot\text{g}^{-1}$, average pore diameter = 1000 Å). They are referred to as Ni/XOA400 and Ni/XO30LS, respectively.

Nickel nitrate ($\text{Ni}(\text{NO}_3)_2\cdot 6\text{H}_2\text{O}$) was provided by Aldrich (purity $> 99.0\%$).

Chemical analyses of the samples were performed by inductive coupling plasma in the center of chemical analysis of the CNRS (Vernaison, France). In the following, the Ni sample weight loading is expressed in wt % of Ni per g of sample calcined at 1000 °C:

$$\text{wt \% Ni} = \frac{M_{\text{Ni}}}{M_{\text{NiO}} + M_{\text{SiO}_2}} \times 100$$

The maximum Ni loading (wt % Ni(∞)) is calculated considering that the overall Ni in solution has precipitated. In the standard conditions of preparation described above, wt % Ni(∞) is equal to 45.5%.

The yield of Ni(II) deposition–precipitation is defined as follows:

$$\text{yield (\%)} = \frac{\text{wt \% Ni}}{\text{wt \% Ni}(\infty)} \times 100$$

The changes in the Ni loading and in the DP Ni(II) yield versus the DP time are reported in Table 2. It may be noted that after 16 h of DP nearly all the Ni(II) has precipitated on silica, so that beyond this time, the sample is aging.

2. Characterization Techniques. The samples were reduced by temperature-programmed reduction (TPR) in a quartz gas flow reactor, from room temperature to 900 °C, with a

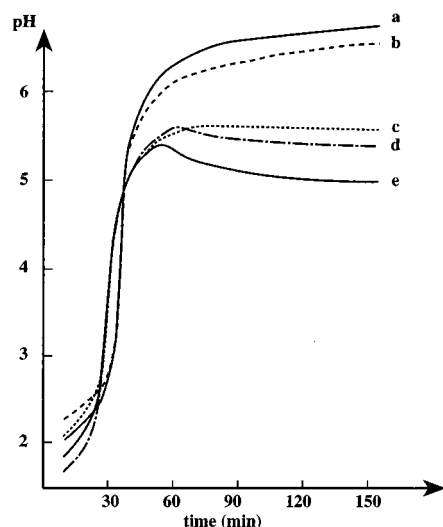


Figure 3. pH curves versus time (up to 150 min) of urea hydrolysis at 90 °C in the presence of (a) urea (0.42 M), nitric acid (0.02 M); (b) urea (0.42 M), nitric acid (0.02 M), silica XOA400 (7.6 g·L⁻¹); (c) urea (0.42 M), nitric acid (0.02 M), nickel nitrate (0.14 M); (d) urea (0.42 M), nitric acid (0.02 M), nickel nitrate (0.14 M), silica XO30LS (7.6 g·L⁻¹); (e) urea (0.42 M), nitric acid (0.02 M), nickel nitrate (0.14 M), silica XOA400 (7.6 g·L⁻¹).

TABLE 2: Change in Ni Loading and in DP Ni(II) Yield versus the DP Time under Standard Conditions and for Other Urea Concentrations

DP time	Ni/XOA 400		Ni/XO30LS	
	wt % Ni	yield (%)	wt % Ni	yield (%)
70 min	5.2	11.4	2.8	6.1
150 min	17.2	37.8	12.5	27.5
4 h	25.1	55.1	21.3	46.8
8 h	35.8	78.7	31.2	68.6
16 h	44.6	98.0	40.8	89.7
24 h	45.4	99.8	42.1	92.5
50 h	44.2	97.1	42.8	94.0
100 h	42.8	94.0	45.4	99.8

heating rate of 7.5 °C·min⁻¹, under 5% v/v H₂ in argon (total flow rate = 25 mL·min⁻¹) at atmospheric pressure. The intensities of the TPR profiles are expressed in arbitrary units. However, for each set of experiments, the same sample weight (40 mg) and the same attenuation of the thermal conductivity detector were used.

The XRD spectra were registered on a Siemens diffractometer (D5000) using Cu Kα radiation. The phase identifications were performed by comparison with the tabulated JCPDS *d*-spacing files.

The IR spectra were scanned (five scans) at room temperature with a FTIR Perkin-Elmer 1750 spectrophotometer. The Ni(II) precipitate samples were finely ground and dispersed in KBr pellets with a ratio of about 1 mg per 100 mg of KBr. The resolution of the IR spectra is 4 cm⁻¹.

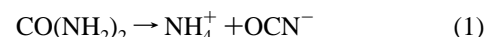
III. Results and Discussion

1. Changes in pH of Various Solutions during Urea Hydrolysis. Before studying the changes in pH of solutions during deposition–precipitation, blank experiments have been performed with various solutions. Figure 3 shows the changes in pH of different solutions containing urea versus the time of urea hydrolysis at 90 °C up to 150 min.

a. Solution Containing Diluted Nitric Acid. Urea hydrolysis at 90 °C in an aqueous solution of nitric acid (0.02 M) (Figure

3a) induces an increase in pH, fast at the beginning because of the neutralization of nitric acid by the OH⁻ ions released, then moderate.

Indeed, thermal decomposition of urea leads to the formation of cyanate and ammonium ions⁸



In acidic solution, the hydrolysis of urea can be written as



and in neutral or basic solution as

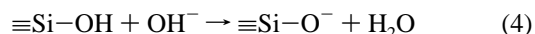


Isocyanate NCO⁻ ions may be considered as intermediate species in the reaction of urea hydrolysis and the limiting step of urea hydrolysis is reaction 1.⁸ The rate of hydroxide ions formation depends on the solution pH (eqs 2 and 3).

b. Solution Containing Diluted Nitric Acid and Silica in Suspension. In the presence of silica XOA400 (Figure 3b), the pH curve passes through a lower pH than the former one (Figure 3a).

It is well-known that silica solubility and dissolution rate depend on particle size, surface area, hydration state, and impurities in silica, as well as composition, temperature, and pH of the solution.⁹ Silica solubility increases with temperature and pH. In pure water, it varies between (1 and 2.5) × 10⁻³ mol·L⁻¹ at room temperature. The dissolution rate increases with both pH and surface area. Iler⁹ has proposed a mechanism of silica dissolution in basic medium (Figure 4), which involves OH⁻ ions as catalysts of silica depolymerization; indeed, for pH lower than 11, the Si(OH)₅⁻ species released is hydrolyzed into silicic acid Si(OH)₄ and the OH⁻ ions are regenerated (Figure 4).

It may be noted that silica exhibits cation exchange properties at pH higher than the IEP (≈2), i.e., as in the present case



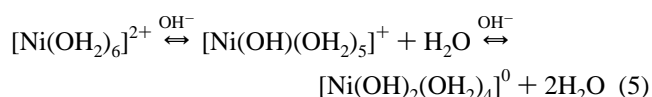
and that the cation exchange capacity increases during dissolution since new silanol groups are generated⁹ (Figure 4).

In basic medium, Si(OH)₄ units can condense, be ionized [SiO(OH)₃]⁻, and form different types of monomeric, oligomeric, and polymeric chains negatively charged. All these species are involved in the equilibrium of depolymerization–polymerization of silica.

Hence, the lower pH of the curve in the presence of silica (Figure 3b) is attributed to the higher consumption of OH⁻ ions because of both the ionization (eq 4) and the dissolution of silica (Figure 4).

c. Solution Containing Diluted Nitric Acid and Nickel Nitrate. With a solution containing urea, nickel nitrate, and nitric acid (Figure 3c), the pH increases fast at the beginning and then reaches a plateau at pH_{plt} = 5.6.

It is well-known that [Ni(OH)₂]₆²⁺ does not exhibit acidic behavior, so a base such as OH⁻ must be added to initiate hydrolysis.¹⁰ Two nickel hydroxo-aqua complexes may then be generated:



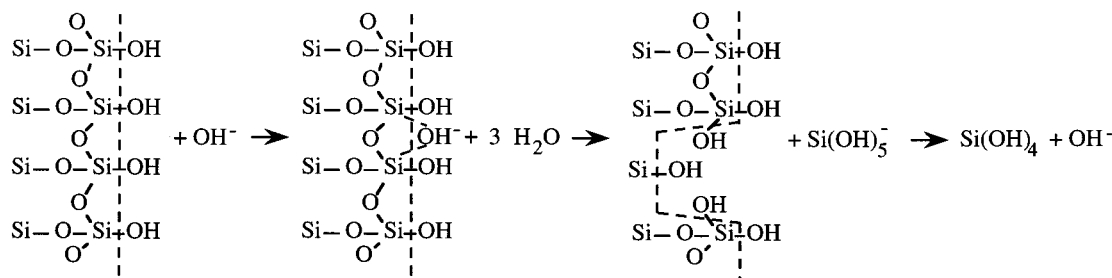
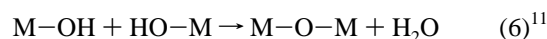


Figure 4. Mechanism of silica dissolution in basic medium.

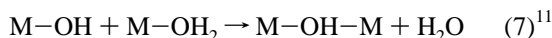
Condensation reactions start as soon as hydroxo ligands appear in the coordination sphere. Two types of condensation reactions exist:

(1) oxolation, i.e., formation of an “oxo” bridge between two metal centers:



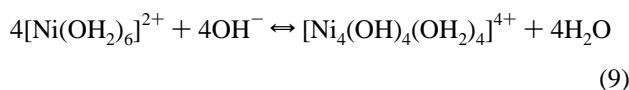
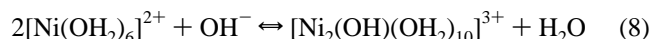
Such a condensation reaction is usually observed when no aqua ligand is available in the coordination sphere of a metal complex.^{12–14} Typically, this reaction occurs with oxo–hydroxo precursors.

(2) olation, i.e., formation of a hydroxo or “ol” bridge between two metal centers:

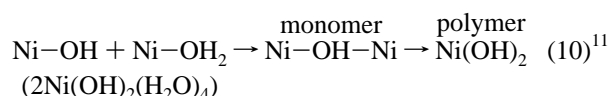


For coordinatively saturated metal hydroxo/aqua complexes, this reaction passes through a nucleophilic substitution where $\text{M}-\text{OH}$ is the nucleophile and OH_2 the leaving group.^{12,13}

Charged precursors cannot condense indefinitely to form a solid phase. In the case of the nickel hexaqua complex, the condensation reactions stop at the tetramer:^{12,15}



In contrast, zero-charged precursors, such as $\text{Ni}(\text{OH})_2(\text{H}_2\text{O})_4$ (eq 5), are able to form a solid phase through infinite condensation of “ol” groups. The final term of this process is the formation of nickel hydroxide:



Hence, the plateau at $\text{pH}_{\text{plt}} = 5.6$ probably arises from the consumption of OH^- ions owing to the shift to the right of the hydrolysis equilibrium of nickel hexaqua complexes (eq 5) arising from the consumption of the hydroxo/aqua complexes for the $\text{Ni}-\text{OH}-\text{Ni}$ ololation/polymerization and the precipitation of nickel hydroxide in solution (eq 10). As shown in a previous paper,⁵ this nickel hydroxide is a turbostratic nickel hydroxide, $\alpha\text{-Ni}(\text{OH})_2$, containing nitrate and isocyanate ions in the interlayers.

2. Changes in pH and in the Nature of the Supported Ni(II) Phase during Deposition–Precipitation. *a. Standard Conditions.* In the standard conditions of deposition–precipitation used in the previous paper⁵ and recalled in the Experimental Section, the pH curve roughly exhibits the same shape for the silicas of low (XO30LS) and high surface area (XOA400)

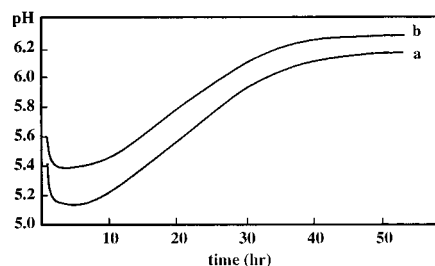


Figure 5. pH curves versus time (up to 50 h) of urea hydrolysis at 90 °C in the presence of (a) urea (0.42 M), nitric acid (0.02 M), nickel nitrate (0.14 M), silica XOA400 (7.6 g·L⁻¹); (b) urea (0.42 M), nitric acid (0.02 M), nickel nitrate (0.14 M), silica XO30LS (7.6 g·L⁻¹).

(Figure 3d,e): at once, pH increases rapidly, passes through a maximum, and then stabilizes at a lower pH. It can be noted that nickel hydroxide (Table 1) precipitates on silica XO30LS (Figure 3d) at lower pH ($\text{pH}_{\text{plt}} = 5.4$) than in solution ($\text{pH}_{\text{plt}} = 5.5$) (Figure 3c), and that nickel phyllosilicate (Table 1) precipitates on silica XOA400 (Figure 3e) at lower pH ($\text{pH}_{\text{plt}} = 5.0$) than nickel hydroxide on XO30LS (Figure 3d). In addition, the maximum of pH is lower and is reached earlier with XOA400 than with XO30LS ($\text{pH}_{\text{max}} = 5.4$ and 5.6 and $t_{\text{max}} = 50$ and 60 min, respectively).

The same pH curves with the same differences have been obtained with nonporous silicas of the same high surface area (AD380, Degussa; $S_{\text{BET}} = 380 \text{ m}^2\cdot\text{g}^{-1}$) and low surface area (OX50, Degussa; $S_{\text{BET}} = 50 \text{ m}^2\cdot\text{g}^{-1}$).

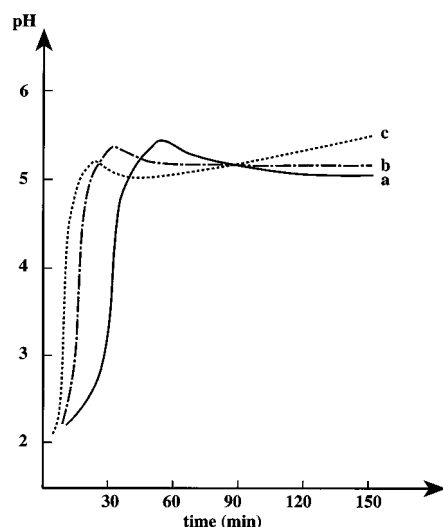
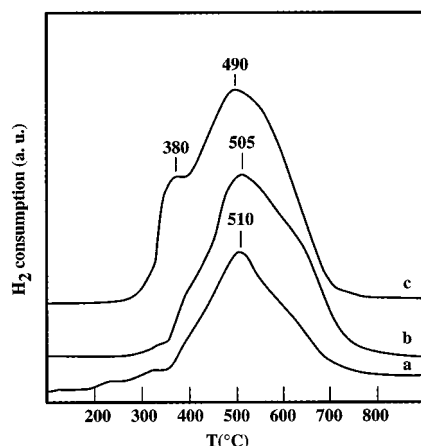
It can be noted that beyond about 8 h of DP, pH increases again (Figure 5).

b. Influence of the Urea Concentration. When the starting urea concentration is higher (0.84; 1.68 M) than that used in standard conditions (0.42 M), the Ni loading increases in the samples (Table 3) in agreement with the results of Richardson and Dubus obtained with the same system.¹⁶ For a urea concentration of 1.68 M, a large fraction of the Ni(II) is precipitated ($\approx 74\%$) after 150 min of DP. The pH curve also depends on urea concentration (Figure 6); both t_{max} and pH_{max} shift to lower values when the concentration increases, and the pH curves cross that obtained in standard conditions. Hence, for 0.84 M of urea, $\text{pH}_{\text{plt}} (=5.1)$ (Figure 6b) is at a slightly higher pH value than for 0.42 M ($\text{pH}_{\text{plt}} = 5.0$) (Figure 6a), and for 1.68 M of urea, pH increases again after the peak of pH and does not reach a plateau within the 150 min of the experiment (Figure 6c).

The TPR profiles of these Ni/XOA400 (150 min) samples exhibit a broad peak at about 500 °C and a shoulder or a peak at 380 °C (Figure 7). According to our previous paper,⁵ the peak at 380 °C arises from the reduction of supported nickel hydroxide (unsupported nickel hydroxide is reducible at about 300 °C), while the peak at 500 °C is due to the reduction of nickel phyllosilicate. Compared to standard conditions (0.42 M) (Figure 7a), the shoulder at 380 °C is more visible on the

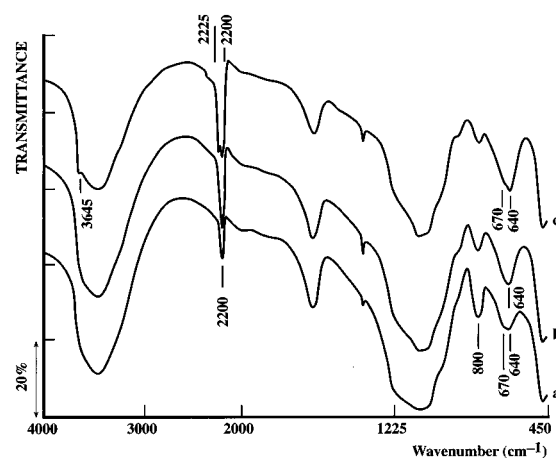
TABLE 3: Changes in Ni Loading, DP Ni(II) Yield, and Nature of the Ni(II) Phase versus Different Preparation Parameters after 150 min of Deposition–Precipitation (Standard Conditions: Bold Characters)

silica	reactant concentrations			Ni loading (wt %)	yield (%)	DP Ni(II) phase
	silica (g·L ⁻¹)	Ni(NO ₃) ₂ ·6H ₂ O (M)	urea (M)			
XOA400	7.6	0.14	0.42	17.2	37.8	1:1 nickel phyllosilicate
	7.6	0.14	0.84	24.6	54.1	1:1 nickel phyllosilicate
	7.6	0.14	1.68	33.9	74.5	1:1 nickel phyllosilicate + Ni(OH) ₂
	7.6	0.015	0.42	7.8	77.2	1:1 nickel phyllosilicate (higher crystallinity)
	7.6	0.07	0.42	15.9	49.5	1:1 nickel phyllosilicate
	7.6	0.14	0.42	17.2	37.8	1:1 nickel phyllosilicate
	3.8	0.14	0.42	27.8	48.3	1:1 nickel phyllosilicate (higher crystallinity)
	7.6	0.14	0.42	17.2	37.8	1:1 nickel phyllosilicate
	15.2	0.14	0.42	9.6	30.0	1:1 nickel phyllosilicate + Ni(OH) ₂
XO30LS	7.6	0.14	0.42	12.5	27.5	Ni(OH)₂ + 1:1 nickel phyllosilicate
	60	0.14	0.42	4.3	38.6	1:1 nickel phyllosilicate

**Figure 6.** Influence of the urea concentration on the pH curves during nickel deposition precipitation in the presence of silica XOA400 (7.6 g·L⁻¹), nickel nitrate (0.14 M), nitric acid (0.02 M): (a) 0.42 M; (b) 0.84 M; (c) 1.68 M.**Figure 7.** Influence of the urea concentration on the TPR profiles of Ni/XOA400 samples prepared by deposition–precipitation for 150 min: (a) 0.42 M; (b) 0.84 M; (c) 1.68 M.

sample prepared with 0.84 M of urea (Figure 7b) and becomes a peak on the sample prepared with 1.68 M of urea (Figure 7c). These changes indicate the formation of a higher proportion of nickel hydroxide when urea concentration increases.

The presence of a mixture of nickel hydroxide and 1:1 nickel phyllosilicate when urea concentration is high (0.84 and 1.68 M) is also attested by the IR spectra (Figure 8). The interpreta-

**Figure 8.** Influence of the urea concentration on the IR spectra of Ni/XOA400 samples prepared by deposition–precipitation during 150 min: (a) 0.42 M; (b) 0.84 M; (c) 1.68 M.

tion of this type of IR spectra was previously given.⁵ The most relevant feature in the IR spectrum of Ni/XOA400 (150 min) prepared in standard conditions (0.42 M of urea) (Figure 8a) is the vibration band with a maximum between 670 and 640 cm⁻¹. It is due to the superimposition of the δ_{OH} vibration of α -Ni(OH)₂ at 640 cm⁻¹ and the δ_{OH} of ill-crystallized 1:1 nickel phyllosilicate at 670 cm⁻¹. Previous EXAFS and TPR studies⁵ have shown that in such a case, the proportion of nickel hydroxide in nickel phyllosilicate was less than 10%. For the samples prepared with higher urea concentration (0.84 and 1.68 M) (Figure 8b,c), the IR band at 640 cm⁻¹ is stronger than that at 670 cm⁻¹, indicating the presence of a higher proportion of α -Ni(OH)₂.⁵ The increasing amount of nickel hydroxide is also confirmed by the presence of a better resolved ν_{OH} vibration band at 3645 cm⁻¹ (Figure 8c) and by the splitting of the isocyanate band at 2200 cm⁻¹. Indeed, the splitting into two bands at 2200 and 2225 cm⁻¹ has been previously attributed to isocyanates located in 1:1 nickel phyllosilicates and nickel hydroxide, respectively.⁵

These samples have also been studied by XRD after 150 min of DP (Figure 9). The bands at 7.25, 2.66, and 1.54 Å, characteristic of the 001, 10, and 11 reflections of a turbostratic nickel hydroxide,⁵ increase in intensity with urea concentration and confirm the formation of an increasing proportion of nickel hydroxide. It can be noted that after 150 min of deposition–precipitation the 1:1 nickel phyllosilicates are too ill-crystallized to provide a diffraction pattern.⁵

All these results show that the higher the urea concentration, the larger the proportion of nickel hydroxide in the DP Ni(II)

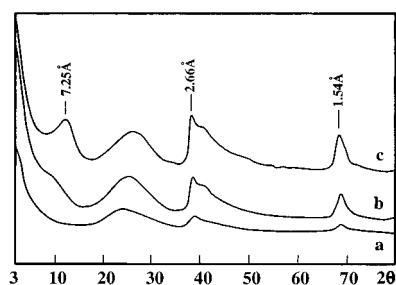


Figure 9. Influence of the urea concentration on the XRD patterns of Ni/XOA400 samples prepared by deposition–precipitation for 150 min: (a) 0.42 M; (b) 0.84 M; (c) 1.68 M.

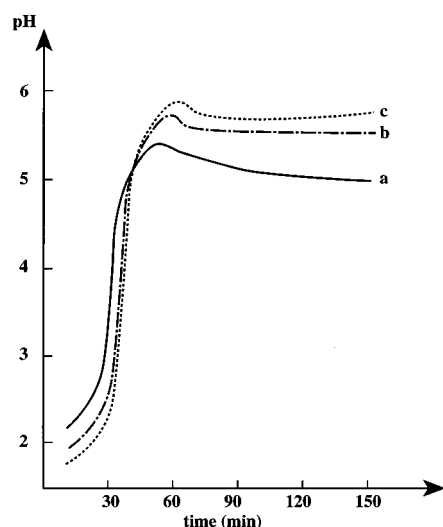


Figure 10. Influence of the nickel nitrate concentration on the pH curves during deposition–precipitation in the presence of silica XOA400 (7.6 g·L⁻¹), urea (0.42 M), nitric acid (0.02 M), and different nickel nitrate concentrations: (a) 0.14 M; (b) 0.07 M; (c) 0.015 M.

phase. However, 1:1 nickel phyllosilicate remains the main species in these samples, as attested by the TPR results.

c. Influence of the Concentration of Nickel Nitrate. The Ni loading in the samples decreases with the starting nickel nitrate concentration (0.14 M (standard conditions), 0.07 and 0.015), whereas the DP Ni(II) yield increases (Table 3). The pH curves exhibit the same shape (Figure 10) but are shifted toward higher pH when the starting nickel concentration decreases.

The TPR profiles obtained for the different nickel nitrate concentrations do not differ significantly (Figure 11), indicating that the same DP Ni(II) phase is formed, i.e., 1:1 nickel phyllosilicate.⁵ However, the maximum of the peak shifts from 500 to 540 °C when the nickel nitrate concentration and the Ni loading decrease, indicating an increasing crystallinity of the 1:1 nickel phyllosilicate.¹⁷ This is in agreement with an observation of Mizutani et al.:¹⁸ the crystallinity of bulk nickel phyllosilicate increases when the OH⁻/Ni²⁺ molar ratio increases.

Hence, the concentration of nickel does not have a strong influence on the nature of the DP Ni(II) phase: 1:1 nickel phyllosilicate is obtained, but its crystallinity improves when the concentration decreases.

d. Influence of the Silica Loading. When the loading of silica XO30LS (60 g·L⁻¹) is high, the pH curve (Figure 12a) is closer to that obtained with silica XOA400 (7.6 g·L⁻¹) (Figure 12b) than to that obtained with silica XO30LS (7.6 g·L⁻¹, standard conditions) (Figure 12c). It can also be noted that (i) the overall surface area developed by 60 g·L⁻¹ of silica XO30LS (44 m²·g⁻¹ × 60 g·L⁻¹) is equal to that of 7.6 g·L⁻¹ of silica

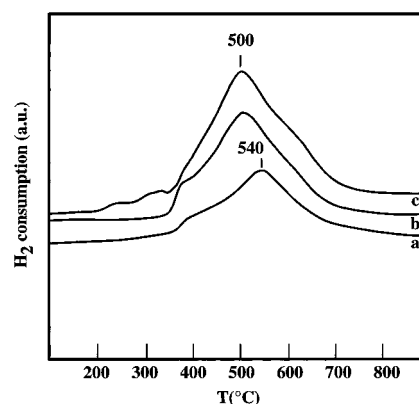


Figure 11. TPR profiles of DP Ni/XOA400 prepared with silica XOA400 (7.6 g·L⁻¹), urea (0.42 M), nitric acid (0.02 M) and different nickel nitrate concentrations, for 150 min of DP time: (a) 0.015 M; (b) 0.07 M; (c) 0.14 M.

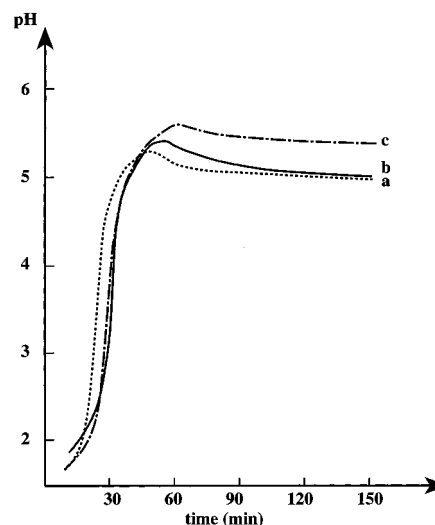


Figure 12. Influence of the silica charge on the pH curves during urea hydrolysis at 90 °C in the presence of nickel nitrate (0.14 M), urea (0.42 M), nitric acid (0.02 M) and different silica concentrations: (a) silica XO30LS (60 g·L⁻¹); (b) silica XOA400 (3.8, 7.6 or 15.2 g·L⁻¹); (c) silica XO30LS (7.6 g·L⁻¹).

XOA400 (356 m²·g⁻¹ × 7.6 g·L⁻¹); (ii) the DP Ni(II) yield is the same (Table 3), indicating that the kinetics of deposition–precipitation is also the same; (iii) the Ni loading is lower after 150 min of DP (4.3 wt % Ni) than in Ni/XOA400 (24.6 wt % Ni), which is consistent with the higher silica loading. If one compares now Ni/XO30LS (60 g·L⁻¹) with Ni/XO30LS (7.6 g·L⁻¹), its Ni loading is also lower but its yield is higher (Table 3); i.e., the kinetics of DP is faster. Its TPR profile (Figure 13b) is different from that of Ni/XO30LS (7.6 g·L⁻¹) (Figure 13a) and of Ni/XOA400 (7.6 g·L⁻¹) (Figure 13c). It exhibits two broad peaks at 440 and 500 °C. The peak at 500 °C can be attributed to 1:1 nickel phyllosilicate.⁵ The one at 440 °C is too different from that obtained with Ni/XO30LS (7.6 g·L⁻¹) at 380 °C (Figure 13a) to be attributed to the reduction of supported nickel hydroxide.⁵ The low Ni loading does not allow one to go further in the characterization of the DP Ni(II) phase by IR spectroscopy.

When the silica XOA400 loading increases in the starting suspension (3.8, 7.6—standard conditions, 15.2 g·L⁻¹), the pH curves are superimposable (Figure 12b). However, the Ni loading in the samples and the DP Ni(II) yield decrease (Table 3). In addition, the DP Ni(II) phases are slightly different since a small amount of nickel hydroxide is formed with the silica

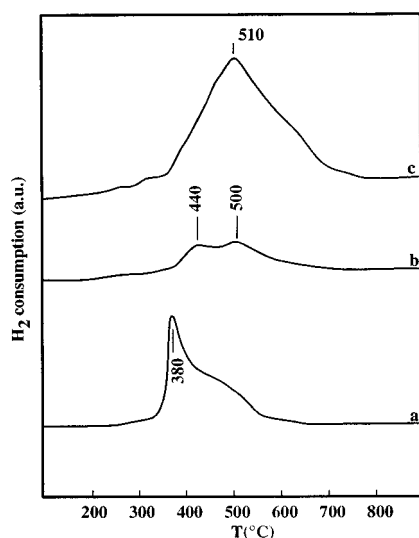


Figure 13. TPR profiles of DP Ni/SiO₂ prepared with nickel nitrate (0.14 M), urea (0.42 M), nitric acid (0.02 M), and different silica concentrations, for 150 min of DP time: (a) 7.6 g·L⁻¹ of silica XO30LS; (b) 60 g·L⁻¹ of silica XO30LS; (c) 7.6 g·L⁻¹ of silica XOA400.

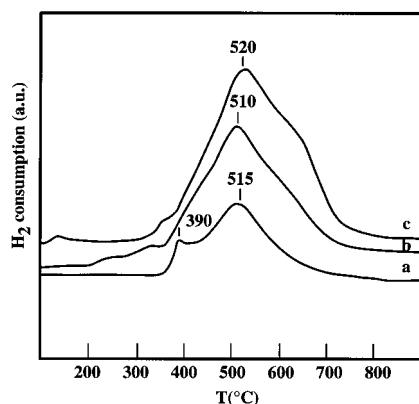


Figure 14. TPR profiles of DP Ni/XOA400 prepared with nickel nitrate (0.14 M), urea (0.42 M), nitric acid (0.02 M) and different silica concentrations, for 150 min of DP time: (a) 15.2 g·L⁻¹; (b) 7.6 g·L⁻¹; (c) 3.8 g·L⁻¹.

loading of 15.2 g·L⁻¹ and better crystallized 1:1 nickel phyllosilicate is obtained with the silica loading of 3.8 g·L⁻¹ than with that of 7.6 g·L⁻¹ (Figure 14).

3. The Formation of Nickel Phyllosilicate. Before discussing these results, it is worthwhile to recall the current knowledge about the formation of nickel phyllosilicates.

There are two types of layered nickel silicates:

1. 1:1 nickel phyllosilicate or serpentine (Si₂Ni₃O₅(OH)₄), also called Ni-lizardite or nepouite when the layers are planar (Figure 2a), Ni-antigorite when the layers are splintery, and Ni-chrysotile when they are curled into cylindrical rolls;

2. 2:1 nickel phyllosilicate whose structural formula is Si₄-Ni₃O₁₀(OH)₂ when it is well-crystallized; it is also called Nitalc or willemseite (Figure 2b).

These structures are well-known and have been extensively described in the literature.¹⁹ A layer of 1:1 nickel phyllosilicate consists of a brucite-type sheet containing Ni(II) in octahedral coordination and a sheet containing linked tetrahedral SiO₄ units (Figure 2a). In 2:1 nickel phyllosilicates, two sheets of linked SiO₄ units sandwich the brucite-type sheets (Figure 2b). The layers are usually neutral and do not exhibit ion-exchange properties.

In contrast with the structure, the mechanism of formation of phyllosilicates is not well-established. Siffert et al.²⁰ found

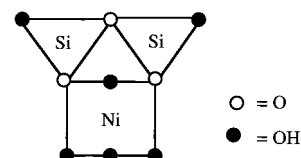
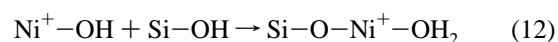
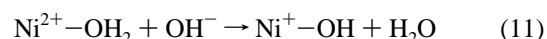


Figure 15. Schematic representation of a building unit of 1:1 nickel phyllosilicate.

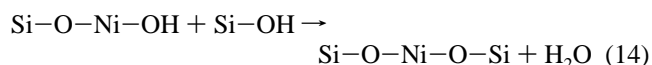
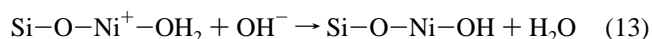
TABLE 4: Free Energy of Formation of 1:1 and 2:1 Nickel Phyllosilicates and Nickel Hydroxide in Aqueous Solution

nickel compound	ΔG°_f (kcal·mol ⁻¹)	ref
1:1 nickel phyllosilicate	-690	24-26
2:1 nickel phyllosilicate	-1040	24-26
nickel hydroxide	-1870	27

that the prerequisites for the formation of phyllosilicates are the followings: (i) silicic species in solution must be monomeric; (ii) metal hydroxo complexes must be present in solution; (iii) the pH must be lower than that of the hydroxide precipitation. The mechanism proposed is based on the formation of two types of monomeric species in solution, depending on the M:Si ratio: monomer I [(HO)₃Si]-O-[M(H₂O)₄(OH)] and monomer II [(HO)₃Si]-O-[M(H₂O)₄]-O-[Si(OH)₃], whose polymerization would lead to the formation of 1:1 and 2:1 phyllosilicates, respectively. More recent works by Mizutani et al.^{18,21} gave better insight into the step of monomer formation in a study on the synthesis of nickel phyllosilicate performed by addition of sodium hydroxide to a solution containing sodium orthosilicate (Na₄O₄Si) and nickel chloride. Since according to Mizutani et al.^{18,21} nickel aqua complex is more acidic than silicic acid, they proposed that the hydrolysis equilibrium of nickel aqua complex (eq 5) is established prior to that of silicic acid and followed by a condensation reaction with silicic acid so as to lead to monomer I:¹⁸



With an excess of silicic acid, monomer I can lead to monomer II via a second condensation reaction:¹⁸



The formation of monomers I and II has not experimentally been proven, and the subsequent steps of polymerization that lead to phyllosilicates are not described in the literature. To the best of our knowledge, the smallest phyllosilicate entity that has been identified, is a 15 Å diameter particle that already contains several building units according to Decarreau²² (Figure 15).

Several authors^{18,21,23,24} showed that the Ni/Si molar ratio in the starting mixture determines the nature of the nickel phyllosilicate. When the Ni/Si ratio is higher than 1.5, 1:1 nickel phyllosilicate (Si₂Ni₃O₅(OH)₄) is formed, whereas when it is equal to 0.5–0.75, 2:1 nickel phyllosilicate (Si₄Ni₃O₁₀(OH)₂) is obtained. The formation of 2:1 nickel phyllosilicate is thermodynamically favored over that of 1:1 nickel phyllosilicate (Table 4).

It may be also mentioned that the Ni–O–Si reactions of condensation (eqs 12 and 14) are oxolation-type reactions (eq 6). However, according to Henry,²⁸ it is more adequate to use

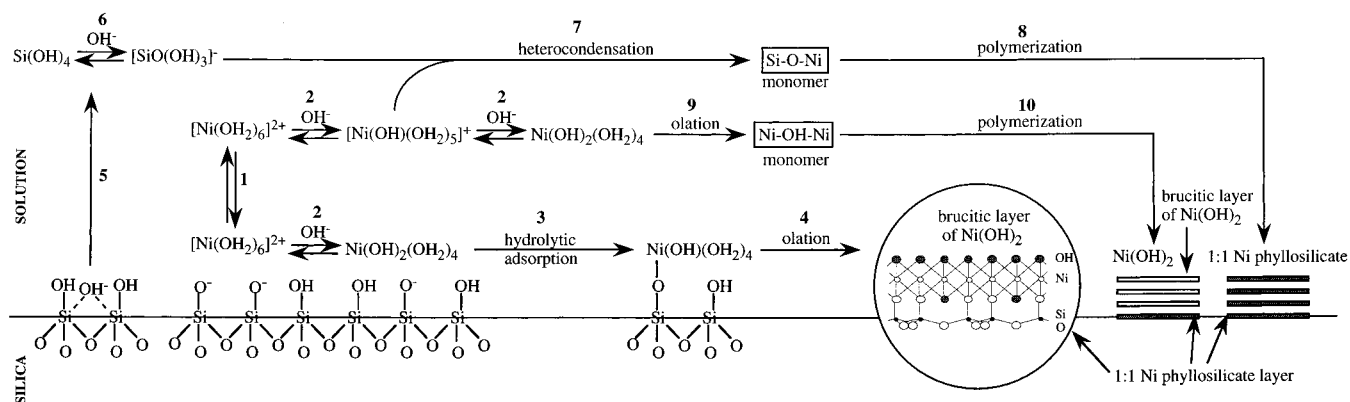
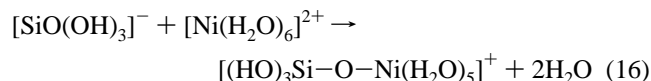
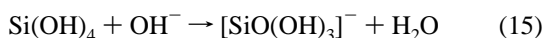


Figure 16. Proposed mechanism for the deposition–precipitation of Ni(II) on silica. For the sake of clarity, when OH[−] reacts, the H₂O produced is not indicated.

the term “heterocondensation” since the condensation reaction involves a Si complex condensing by oxolation and a Ni complex condensing by ololation. In addition, the claim of Mizutani et al.^{18,21} that nickel aqua complex is more acidic than silicic acid is not obvious since the hydrolysis constant pK_1 depends on the ionic strength and the temperature of the solution, and the pK_1 of Si(OH)₄ can vary between 8 and 10,²⁹ while that of Ni(H₂O)₆ varies between 9.2 and 10.9 (ionic strength $I = 0$) and 6.5–10.2 ($I > 0$).³⁰ Henry³¹ proposes another mechanism of heterocondensation than that of Mizutani et al. (eqs 11 and 12):^{18,21} when a positively charged complex such as [Ni(H₂O)₆]²⁺ moves toward a neutral species such as Si(OH)₄, the electrostatic repulsion between the positive charge and the protons of Si(OH)₄ favors the ionization of the latter. In consequence, the following equations are proposed by Henry:³¹



Like for ololation reaction (eq 7), heterocondensation kinetics is governed by a nucleophilic attack. Since [SiO(OH)₃][−] is a better nucleophile than [Ni(OH)(H₂O)₅]⁺ or Ni(OH)₂(H₂O)₄, it will condense faster with [Ni(H₂O)₆]²⁺. Hence, the following kinetics order can be deduced: heterocondensation > ololation. In other words, the kinetics of nickel phyllosilicate formation is expected to be faster than that of nickel hydroxide formation. This is in agreement with the experimental results mentioned above: the entity detected within the first seconds of nickel phyllosilicate synthesis is already a phyllosilicate and not an hydroxide.

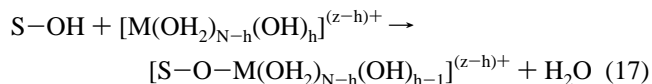
IV. Proposed Model for the Mechanism of Deposition–Precipitation of the Ni(II) Phase on Silica

To explain the changes observed in the nature of the Ni(II) phase formed on silica during deposition–precipitation in standard conditions as a function of the DP time and the support surface area (Table 1), a mechanism can be proposed.

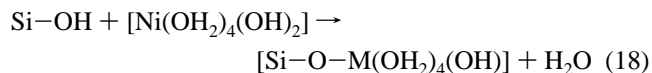
At the beginning of the basification of the solution, silica is negatively charged and exhibits cation exchange capacity since $\text{pH} > \text{IEP} \approx 2$ (eq 4). As a consequence, the first step of deposition–precipitation is probably an electrostatic adsorption of the Ni(II) hexaqua complexes on the silica support (step 1 in Figure 16). The Ni(II) hexaqua complexes are in equilibrium with [Ni(OH)(OH₂)₅]⁺ and Ni(OH)₂(OH₂)₄ (eq 5 and step

2 in Figure 16). The Ni(II) hydroxo aqua complexes close to the silica surface can react with the silanol groups via an hydrolytic adsorption (step 3).

Indeed, according to Marcilly and Franck,³² when metal aqua complexes are hydrolyzed and form hydroxo aqua or oxohydroxo complexes in basic medium (eq 5), the so-called hydrolytic adsorption can occur on the oxide support, providing that the latter contains surface hydroxyl groups:



According to these authors,³² this reaction is of the same nature as the condensation reactions occurring during hydroxide precipitation. Since, only zero-charged precursors can form a solid phase through infinite condensation reaction (Section III.1.c), we rather suggest that this reaction occurs between the zero-charged nickel complex and the oxide support:



It can be noted that the hydrolytic adsorption is an heterocondensation reaction.

The Ni(II) hydroxo aqua complexes can also react with each other via ololation reaction (eq 7) and form a brucitic layer of octahedral Ni(II) bonded to the silica surface (step 4). This brucitic layer bonded to silica can also be considered as a sheet of 1:1 nickel phyllosilicate (Figure 2a) at the support–solution interface. Meanwhile, silica starts to dissolve and silicic acid to be released in solution (see Section III.1.b, and steps 5 and 6). At this point, two features may happen, depending on the amount of released Si(OH)₄, which depends on the silica surface area and the DP time:

For silica of high surface area (XOA400), the dissolution is kinetically favored because of the large support–solution interface (see Section III.1.b). Hence, the amount of silicic species is large enough to react with the nickel complexes in solution via heterocondensation reaction and form Si–O–Ni monomers (step 7). Further polymerization to form layers of 1:1 nickel phyllosilicate (step 8) and growth on the brucitic layer of Ni(II) bonded to silica lead to the formation of supported 1:1 nickel phyllosilicates.

The solubility of silica of low surface area (XO30LS) is lower and its rate of dissolution is slower because of the smaller support–solution interface. Therefore, the amount of Si(OH)₄ is low at the beginning of the deposition–precipitation (≤ 4 h).

So, Si—O—Ni heterocondensation is a minor reaction, and ololation between the $\text{Ni}(\text{OH})_2(\text{OH}_2)_4$ complexes is the main reaction (eq 7 and step 9). Further polymerization to form brucitic layers of Ni(II) (step 10) and growth on the brucitic layer of Ni(II) bonded to silica lead to the formation of supported nickel hydroxide.

It can be noted that the brucitic layer of Ni(II) bonded to silica acts as nuclei for the growth of supported 1:1 nickel phyllosilicate or supported nickel hydroxide.

V. Consistency of the Mechanism of Deposition—Precipitation

1. With Published Data. The assumption that a layer of 1:1 nickel phyllosilicate arising from the anchoring of a Ni(II) brucitic layer on the silica surface (step 4) acts as a nucleation site for the growth of supported $\text{Ni}(\text{OH})_2$ (step 10) or 1:1 nickel phyllosilicate (step 8) is in agreement with the literature data. Tsvetkov et al.³³ have shown that in the case of Co phyllosilicates, their formation is preceded by ion exchange of metal ions with surface silanol groups. This is confirmed by Ohtsuka et al.,³⁴ who studied the deposition—precipitation of Ni(II) on clay supports by urea hydrolysis. $\text{Ni}(\text{OH})_2$ precipitates uniformly on the external surface of the clay providing that the latter exhibits cation exchange capacity. Conversely, $\text{Ni}(\text{OH})_2$ does not precipitate on the clay surface when the clay does not exhibit cation exchange properties. In addition, de Roos et al.³⁵ have shown that the adherence of the DP Ni(II) phase depends on the hydroxylation state of the support: on quartz pretreated at 1000 °C, a weakly interacting nickel hydroxide is deposited, while in the presence of a mixture of quartz (a few $\text{m}^2\cdot\text{g}^{-1}$) and silica (380 $\text{m}^2\cdot\text{g}^{-1}$) nickel prefers to interact with silica and form nickel phyllosilicate rather than to interact with quartz. Hermans and Geus³ and Coenen³⁶ suggested that at least one monolayer of 1:1 nickel phyllosilicate is present at the interface of attachment between the silica and the hydroxide in DP Ni/SiO₂ samples. According to Coenen, epitaxial growth of $\text{Ni}(\text{OH})_2$ could occur on the nickel silicate sheet. This was confirmed by Ohtsuka et al.,³⁷ who observed the growth of brucitic layers of $\text{Ni}(\text{OH})_2$ parallel to the silicate layers during decomposition of Ni(II) ammine complex at 90–100 °C on silicate-type clay supports.

The formation of supported 1:1 nickel phyllosilicate via Ni—O—Si heterocondensation/polymerization is in competition with that of nickel hydroxide that arises from Ni—OH—Ni ololation/polymerization. The fact that for the silica of low surface area nickel hydroxide is formed at short DP time (<4 h) and 1:1 nickel phyllosilicate after longer time (≥ 4 h) indicates the following:

(i) nickel hydroxide is gradually transformed into 1:1 nickel phyllosilicate (whose formation is thermodynamically favored (Table 4)), probably via a mechanism of $\text{Ni}(\text{OH})_2$ depolymerization/Ni—O—Si heterocondensation/polymerization;

(ii) Ni—O—Si heterocondensation/polymerization reaction is faster than Ni—OH—Ni ololation/polymerization, which confirms what was stated in Section III.3.;

(iii) the formation of 1:1 nickel phyllosilicate, which is thermodynamically favored over that of $\text{Ni}(\text{OH})_2$ (Table 4), is also kinetically favored but is limited by the amount of $\text{Si}(\text{OH})_4$ in solution, i.e., the rate of silica dissolution. It can be noted that the formation of 2:1 nickel phyllosilicate is thermodynamically favored over that of 1:1 nickel phyllosilicate (Table 4) but is kinetically unfavored. Indeed, after 1 month of DP, i.e., a long aging period, 1:1 nickel phyllosilicate is still observed by IR spectroscopy. It is necessary to accelerate the kinetics under hydrothermal treatment (190 °C, 7 days) to observe the

transformation of 1:1 nickel phyllosilicate into 2:1 nickel phyllosilicate.⁵

The mechanism of deposition—precipitation of Ni(II) on silica is also in agreement with the different morphologies of the DP Ni(II) phases observed by TEM in a previous paper:⁵

For short DP time and silica of high surface area ($\approx 400 \text{ m}^2\cdot\text{g}^{-1}$), the formation of a high number of thin platelets of 1:1 nickel phyllosilicate supported on silica can be related to the high cation exchange capacity of this type of silica, which leads to the electrostatic adsorption of a large number of Ni^{2+} ions (step 1 in Figure 16). After hydrolytic adsorption on silica (step 3) and condensation between neighboring Ni(II) species (step 4), many nuclei consisting of Ni(II) brucitic layers bonded to silica are formed. The latter are responsible for the formation of a high number of thin platelets of 1:1 nickel phyllosilicate homogeneously dispersed on the silica support, indicating the formation of a large Ni(II)—silica interface.

In contrast, the formation of a restricted number of large stacks of nickel hydroxide nonhomogeneously dispersed on the silica of low surface area ($\approx 50 \text{ m}^2\cdot\text{g}^{-1}$) may be explained by the lower exchange capacity of the silica, which leads to a smaller number of nuclei of Ni(II) brucitic layers bonded to silica, i.e., a limited number of nucleation sites, and therefore to a smaller Ni(II)—silica interface.

The mechanism of deposition—precipitation is also consistent with the fact that the morphology and distribution of the DP Ni(II) phases depend on the silica structure (porous or nonporous). On nonporous silica of low surface area (OX50, 50 $\text{m}^2\cdot\text{g}^{-1}$), nickel hydroxide better follows the shape of the silica particles than on porous silica (XO30LS, 44 $\text{m}^2\cdot\text{g}^{-1}$).⁵ The large curvature radius of the nonporous silica particles leads to the formation of a more uniform Ni(II) brucitic layer coverage (no geometrical or sterical hindrance), i.e., a larger Ni(II)—silica interface, on which the DP Ni(II) phase can grow more uniformly. This observation may again be related to the fact that the solubility and the rate of solubility of silica depend on the radius of curvature of silica.

2. With the pH Curves. The lower pH observed during Ni(II) deposition—precipitation (in the presence of silica) (Figure 3d,e) than during Ni(II) precipitation (absence of silica) (Figure 3c) and the presence of a maximum of pH associated with a drop can be explained on the basis of the deposition—precipitation mechanism: the consumption of Ni(II) complexes is faster in the presence of silica than in solution because of the formation of the Ni(II) brucitic layer bonded to the silica support (steps 3 and 4 in Figure 16) and because the kinetics of Ni—O—Si heterocondensation is faster than that of Ni—OH—Ni ololation (see Section III.3.). This leads to a more important shift to the right in the equilibrium of hydrolysis of nickel hexaqua complexes (Mizutani's mechanism of heterocondensation, eqs 11 and 12) or of $\text{Si}(\text{OH})_4$ (Henry's mechanism, eqs 15 and 16) (step 2 or 6 in Figure 16) and to the consumption of a higher amount of OH^- ions.

The presence of a maximum of pH and its associated drop is clearly related to the presence of both silica and nickel in solution since when one is missing (Figure 3b or c), they are not observed.

The same type of curves as in Figure 3c,e has been obtained by Hermans and Geus³ in the absence or in the presence of silica of high surface area, respectively. The presence of a peak in the pH curve of deposition—precipitation, which makes one of the differences between deposition—precipitation on silica and precipitation in solution, has been interpreted by these authors to be due to a nucleation barrier: the sudden nucleation

induces a drop in pH because of the OH[−] consumption, after which the growth of the nickel phyllosilicate proceeds at a lower pH level. However, the maximum of pH and the associated drop are absent from the pH curve obtained during the preparation of DP Ni/Al₂O₃,³⁸ although nickel aluminate and most of the nickel hydroxide are deposited–precipitated, i.e., in interaction with the support. Therefore, it can be deduced that the maximum of pH and the associated drop are probably not related to thermodynamics, but to kinetics.

According to Hermans and Geus³, the pH_{pl} value at which deposition–precipitation proceeds is lower than that of the precipitation in solution because the DP Ni(II) phase is less soluble than nickel hydroxide, which precipitates in solution and because it interacts with the surface support (see Introduction). This thermodynamic approach again may be questioned since as mentioned in the next paragraph, the system is not at thermodynamic equilibrium. In addition, for DP time longer than 4 h, i.e., when nickel hydroxide starts to be significantly transformed into 1:1 nickel phyllosilicate on silica XO30LS (Figure 5b), the pH remains the same, i.e., different from that obtained with Ni/XOA400, which also contains Ni phyllosilicates (Figure 5a).

a. pH Curves Obtained with Silicas of Different Surface Areas. The maximum of pH is observed at lower t_{\max} and lower pH_{max}, and the plateau at a lower pH with silica XOA400 (Figure 3e) than with silica XO30LS (Figure 3d). The faster consumption of OH[−] ions during DP on XOA400 than on XO30LS can be explained as follows: (i) more Ni(II) hydroxo-aqua complexes, and so more OH[−] ions, are consumed for the formation of the Ni(II) brucitic layer bonded to the silica surface because of the higher silica surface area; (ii) more Ni(II) hydroxo-aqua complexes (Mizutani's mechanism of heterocondensation, eqs 11 and 12) or [SiO(OH)₃][−] species (Henry's mechanism, eqs 15 and 16) are consumed for the formation of 1:1 nickel phyllosilicate on silica XOA400 than for the formation of nickel hydroxide on silica XO30LS, since the kinetics of 1:1 nickel phyllosilicate formation is faster than that of nickel hydroxide formation as mentioned in Section III.3. This is confirmed by the fact that for short DP times (70 and 150 min) the Ni loading is higher on silica XOA400 than on silica XO30LS (Table 2).

The plateau of the pH curves (Figure 3d,e) possibly arises from the establishment of a dynamic equilibrium between the formation of OH[−] ions by urea hydrolysis and their consumption for the deposition–precipitation of the Ni(II) phase. This equilibrium is transitory and lasts as long as Ni(II) is precipitating. Indeed, beyond about 8 h of DP, when almost all the Ni(II) ions are precipitated on both types of silica (the DP Ni(II) yield reaches 90%, Table 2), pH increases again because urea continues to be hydrolyzed and OH[−] ions continue to be released (Figure 5).

b. pH Curves Obtained with Different Urea Concentrations. Examination of the pH curves (Figure 6) shows that increasing urea concentration (0.42, 0.84 and 1.68 M) increases the rate of basification of the solution since the neutralization of nitric acid occurs faster. The lower t_{\max} and pH_{max} values indicate that increasing urea concentration accelerates the process of deposition–precipitation, which is also confirmed by the increasing DP Ni(II) yield (Table 3).

The fact that the pH curves cross that obtained with 0.42 M of urea, and that pH_{pl} is higher for 0.84 M urea concentration than for 0.42 M, is consistent with the fact that when urea concentration increases, the proportion of nickel hydroxide in the DP Ni(II) phase increases (Figures 7–9), although 1:1 nickel phyllosilicate remains the main species in these samples, as

attested by the TPR results (Figure 7). Hence, higher basification rate leads to a higher concentration of nickel complexes; therefore, the ratio of nickel hydroxo-aqua complexes over silicic species in solution is higher than in standard conditions. As a consequence, Ni–OH–Ni ololation/polymerization is favored over Ni–O–Si heterocondensation/polymerization, which is limited by silica dissolution.

For a concentration of 1.68 M (Figure 6c), pH increases again after the pH peak instead of reaching a plateau, because of the formation of excess of OH[−] ions: OH[−] ions are produced faster than they are consumed, so the transitory dynamic equilibrium between the formation of OH[−] ions by urea hydrolysis and their consumption for the deposition–precipitation of the Ni(II) phase is not reached. As a consequence, the increase in pH that was observed after 8 h of DP in standard conditions (Figure 5) occurs earlier. These results confirm the relevance of the kinetic aspect of the mechanism of deposition–precipitation and of the use of the expression “transitory dynamic equilibrium” for the pH plateau observed under standard conditions. One might have suggested that the excess of OH[−] could have led to Ni(OH)₂ precipitation in solution. However, this compound was not detected by TPR since it would have provided a peak at 300 °C.⁵

c. pH Curves Obtained with Different Nickel Concentrations. The shift of the pH curves toward higher pH when the starting nickel nitrate concentration decreases (0.14, 0.07, and 0.015 M) (Figure 10) is due to the fact that less OH[−] ions are required for the deposition–precipitation. This is in agreement with the decreasing Ni loading in the samples although all the nickel is not precipitated since the DP Ni(II) yield is less than 100% (Table 3). It can be deduced that the kinetics of deposition–precipitation of 1:1 nickel phyllosilicate is slowed by the lower Ni concentration. This interpretation is consistent with the fact that 1:1 nickel phyllosilicate is better crystallized when the Ni concentration decreases (Figure 11).

d. pH Curves Obtained with Different Silica Loadings. When the loading of silica XO30LS (60 g·L^{−1}) is high, the pH curve (Figure 12a) is closer to that observed with silica XOA400 (7.6 g·L^{−1}) (Figure 12b) than to that observed with silica XO30LS (7.6 g·L^{−1}) (standard conditions). The DP Ni(II) yield is also closer to that obtained with silica XOA400 (7.6 g·L^{−1}), and a higher proportion of nickel phyllosilicate is formed (Figure 13b).

These results can be explained as follows: increasing silica loading increases the overall silica surface area, and more Si(OH)₄ are released in solution than with silica XO30LS (7.6 g·L^{−1}), so the kinetics of deposition–precipitation is closer to that of silica XOA400 (7.6 g·L^{−1}) than of to that of silica XO30LS (7.6 g·L^{−1}). It can be noted that the formation of 1:1 nickel phyllosilicate and the higher DP Ni(II) yield are consistent with the higher rate of Si–O–Ni heterocondensation than that of Ni–OH–Ni ololation.

When the silica XOA400 loading increases in the starting suspension (3.8, 7.6—standard conditions, 15.2 g·L^{−1}), the pH curves are almost superimposable (Figure 12b). However, the DP Ni(II) yield decreases (Table 3), indicating that the kinetics of deposition–precipitation is slowed when the silica loading increases. This is also attested by the fact that (i) the TPR profile of Ni/XOA400 (15.2 g·L^{−1}, 150 min, 9.6 wt % Ni) (Figure 14a) looks like that of Ni/XOA400 (7.6 g·L^{−1}, 70 min, 5.2 wt % Ni) reported in ref 5, i.e., the DP Ni(II) phase is the same as that obtained after shorter DP time under standard conditions; (ii) the TPR profile of Ni/XOA400 (3.8 g·L^{−1}, 150 min, 27.8 wt % Ni) (Figure 14c) looks like that of Ni/XOA400

(7.6 g·L⁻¹, 4 h, 25.1 wt % Ni),⁵ i.e., the DP Ni(II) phase is the same as that obtained after longer DP time under standard conditions.

The results can be explained as follows: when the silica loading increases, more OH⁻ are involved in silica deprotonation (eq 4) and dissolution (Figure 4) since more surface hydroxyls are available; therefore, less OH⁻ ions are available for the hydrolysis of [Ni(H₂O)₆]²⁺ (Mizutani's mechanism, eqs 11 and 12) or of Si(OH)₄ (Henry's mechanism, eqs 15 and 16), and the kinetics of deposition–precipitation is slowed. The step of transitory dynamic equilibrium (pH_{pit}) would be probably extended in the first case and shortened in the second one. That means that to change the silica loading is equivalent to changing the DP time under the standard conditions of preparation. However, it is not clear why *t*_{max} and pH_{max} are not affected by the change in the silica loading. It is not clear either why the pH curve changes when the silica XO30LS loading changes and why it does not change when the silica XOA400 loading changes.

VI. Conclusion

In line with our former study on the characterization of the Ni(II) phase deposited–precipitated on silica,⁵ a mechanism of deposition–precipitation is proposed, and summarized in Figure 16. It results from a kinetic competition between two types of reactions:

the Ni–O–Si heterocondensation/polymerization, which leads to the growth of supported 1:1 nickel phyllosilicate on a Ni(II) brucitic layer bonded to silica;

the Ni–OH–Ni ololation/polymerization that leads to the formation of α-Ni(OH)₂, which also grows on a Ni(II) brucitic layer bonded to silica.

The former type of reaction is faster than the latter but is limited by the concentration and diffusion of silicic acid in solution arising from silica dissolution. The brucitic layer of Ni(II) bonded to silica acts as nuclei for the growth of supported 1:1 nickel phyllosilicate or supported nickel hydroxide.

This molecular approach to the mechanism of deposition–precipitation, mainly based on a kinetic competition between these two reactions, differs from the mechanism proposed by Geus,⁴ which is rather based on the kinetic and thermodynamic approach of the nucleation and growth of the DP Ni(II) phase.

The mechanism enables one (i) to explain why nickel hydroxide or nickel phyllosilicate are deposited–precipitated, depending on the silica surface area; (ii) to interpret the changes in the pH curves, the DP Ni(II) yield, and the nature of the DP Ni(II) phase as a function of several parameters of preparation: the concentrations of urea and nickel nitrate and the silica loading.

Acknowledgment. The authors warmly acknowledge Dr. C. Marcilly (Institut Français du Pétrole), Prof. M. Henry (Université de Strasbourg), and Prof. A. Decarreau (Université de Poitiers) for their very useful and helpful discussions. The authors are also indebted to Rhône Poulenc (France) for financial contribution to this work.

References and Notes

- (1) Geus, J. W. Dutch Pat. Appl. 6705,259, 1967; 6813,236, 1968.

- (2) van Dillen, J. A.; Geus, J. W.; Hermans, L. A.; van der Meijden, J. In *Proceedings of the 6th International Congress on Catalysis, London, 1976*; Bond, G. C., Wells, P. B., Tompkins, F. C., Eds.; The Chemical Society: London, 1977; p 677.
- (3) Hermans, L. A. M.; Geus, J. W. In *Preparation of Catalysts II*; Delmon, B., Grange, P., Jacobs, P. A., Poncelet, G., Eds.; Elsevier: Amsterdam, 1979; p 113.
- (4) Geus, J. W. In *Preparation of Catalysts III*; Poncelet, G., Grange, P., Jacobs, P. A., Eds.; Elsevier: Amsterdam, 1983; p 1.
- (5) Burattin, P.; Che, M.; Louis, C. *J. Phys. Chem. B* **1997**, *101*, 7060.
- (6) Génin, P.; Delahaye-Vidal, A.; Protomer, F.; Tekaiia, F.; Figlarz, M. *Eur. J. Solid State Inorg. Chem.* **1991**, *28*, 505.
- (7) Clause, O.; Bonnevot, L.; Che, M.; Dexpert, H. *J. Catal.* **1991**, *130*, 21.
- (8) Shaw, W. H. R.; Bordeaux, J. J. *J. Am. Chem. Soc.* **1955**, *77*, 4729.
- (9) Iler, R. *The Chemistry of Silica*; John Wiley and Sons: New York, 1979.
- (10) Livage, J.; Henry, M. In *Ultrastructure Processing of Advanced Ceramics*; Mackenzie, J. D., Ulrich, D. R., Eds.; John Wiley and Sons: New York, 1988; p 183.
- (11) This simplified formula does not take into account the other ligands and the possible charge of the metal complex.
- (12) Livage, J.; Henry, M.; Sanchez, C. *Prog. Solid State Chem.* **1988**, *18*, 259.
- (13) Brinker, C. J.; Scherer, G. W. *Sol–Gel Science—The Physics and Chemistry of Sol–Gel Processing*; Academic Press: Boston, MA, 1990.
- (14) Jolivet, J. P.; Henry, M.; Livage, J. *De la Solution à l'Oxyde*; InterEditions-CNRS: Paris, 1994.
- (15) Kolski, G. B.; Kjeldahl, N. K.; Margerum, D. W. *Inorg. Chem.* **1969**, *8*, 1211.
- (16) Richardson, J. T.; Dubus, R. T. *J. Catal.* **1978**, *54*, 207.
- (17) Carriat, J. Y.; Che, M.; Kermarec, M.; Decarreau, A. *Catal. Lett.* **1994**, *25*, 127.
- (18) Mizutani, T.; Fukushima, Y.; Kamigaito, O. *Bull. Chem. Soc. Jpn.* **1990**, *63*, 2094.
- (19) Bailey, S. W. In *Crystal Structures of Clay Minerals and their X-ray Identification*; Brindley, G. W., Brown, G., Eds.; Mineralogical Society: London, 1980; p 1.
- (20) Siffert, B. *Mem. Serv. Carte Géol. Alsace Lorraine* **1962**, *21*, 59.
- (21) Mizutani, T.; Fukushima, Y.; Okada, A.; Kamigaito, O. *Bull. Chem. Soc. Jpn.* **1990**, *63*, 618.
- (22) Decarreau, A. *Geochim. Cosmochim. Acta* **1985**, *49*, 1537.
- (23) Martin, G. A.; Renouprez, A.; Dalmai-Imelik, G.; Imelik, B. *J. Chim. Phys.* **1970**, *67*, 1149.
- (24) Mondésir, H. Ph.D. Thesis, Paris-Sud, 1987.
- (25) Tardy, Y.; Garrels, R. M. *Geochim. Cosmochim. Acta* **1977**, *41*, 87.
- (26) Sverjensky, D. A. *Geochim. Cosmochim. Acta* **1977**, *49*, 853.
- (27) Wagman, D. D.; Evans, W. H.; Parker, V. B.; Schumm, R. H.; Halow, I.; Bailey, S. M.; Churney, K. L.; Nuttall, R. L. The NBS tables of chemical thermodynamic properties. Selected values for inorganic and C1 and C2 organic substances in SI units. *J. Phys. Chem. Ref. Data* **1982**, *11* (Suppl. 2), 2–392; American Chemical Society and the American Institute of Physics for the National Bureau of Standards: Washington, DC.
- (28) Henry, M. *Coord. Chem. Rev.*, in preparation.
- (29) Baes, C. F.; Mesmer, R. E. *The Hydrolysis of Cations*; John Wiley and Sons: New York, 1976.
- (30) Burgess, J. *Metal Ions in Solution*; Ellis Horwood Ltd: Chichester, 1978.
- (31) Henry, M. Personal communication.
- (32) Marcilly, C.; Franck, J. P. *Rev. Inst. Fr. Pet.* **1984**, *39*, 337.
- (33) Tsvetkov, V. K.; Pak, V. N.; Aleskovskii, V. B. *Zh. Prikl. Khim.* **1976**, *49*, 984.
- (34) Ohtsuka, K.; Koga, J.; Suda, M.; Ono, M. *J. Am. Ceram. Soc.* **1989**, *72*, 1924.
- (35) de Roos, G.; Fluit, J. M.; Hermans, L. A. M.; Geus, J. W. *Z. Anorg. Allg. Chem.* **1979**, *449*, 115.
- (36) Coenen, J. W. E. *Appl. Catal.* **1989**, *54*, 65.
- (37) Ohtsuka, K.; Koga, J.; Tsunoda, M.; Suda, M.; Ono, M. *J. Am. Ceram. Soc.* **1990**, *73*, 1719.
- (38) Burattin, P. Ph.D. Thesis, Paris VI, 1994.